Appl. Phys. A (2015) 119:783–790
DOI 10.1007/s00339-015-9030-6

Applied Physics A
Materials Science & Processing

Self-assembled growth of tandem nanostructures based on TiO_2 mesoporous/ZnO nanowire arrays and their optoelectronic and photoluminescence properties

Bayram Kılıç · Volkan Çelik

Received: 27 November 2014 / Accepted: 1 February 2015 / Published online: 11 February 2015

Abstract Growth of ZnO nanowires within TiO_2 mesoporous structures is carried out by hydrothermal method. Structural, optical and thermal characterizations have been carried out by SEM, XRD, EDAX, DTG, TG, PL and UV–Vis spectroscopy. XRD characterization shows that the all diffraction peaks of the tandem nanostructures films can be well indexed to a mixture of hexagonal wurtzite ZnO and anatase TiO_2 structures. The UV–Visible absorbance spectrum indicates that the tandem nanostructures based on TiO_2 mesoporous/ZnO nanowire arrays have 3.13 eV band gap energy while pure ZnO nanowire and bare TiO_2 mesoporous show 3.37 and 3.22 eV band gap energy, respectively. The PL spectra of tandem nanostructures show that the UV, violet and yellow emission peaks appeared at 3.1, 2.6 and 2.3 eV, respectively. It has been shown that from the PL spectra, the enhanced ultraviolet emission of TiO_2/ZnO tandem structures is related to the fluorescence resonance energy transfer between TiO_2 mesoporous and ZnO nanowires. Thermogravimetric analysis from room temperature to 800 °C has been performed to identify the thermal stability and the amount of tandem TiO_2/ZnO structures.

1 Introduction

Nanosemiconductor shows a wide range of physical, chemical and optoelectronic properties depending on their surface morphologies [1]. Nanosemiconductor materials draw intensive interests because of their improved properties and promising technological applications, such as photochemical solar cells, photocatalysts, photosensors, electroluminescent displays and biolabels [2]. Mesoporous and nanowires are accepted as ideal system for investigating the transport process in one-dimensional (1D) confined objects, which are useful for understanding the fundamental phenomena in low-dimensional systems and developing new generation nanodevices with high performance [3, 4]. TiO_2 mesoporous and 1D ZnO nanowires have been investigated as a basic model structure for nanoelectronic devices because of their physical properties and their potential applications to serve as a basis for nanoscale devices [5, 6]. ZnO is a low-cost and widely used semiconductor material with prominent physical and chemical characteristics [7]. At room temperature, the band gap and exciton binding energy of ZnO are 3.37 and 60 meV, respectively, both contributing to its extraordinary chemical and thermal stability [8]. Thus, ZnO thin films exhibit magnificent applications in the manufacturing process of nanodevices [9]. 1D ZnO nanowires have also some important advantages. For example, they exhibit both semiconducting and piezoelectric (PZ) properties which can form the basis for electromechanically coupled sensors and transducers [10]. In addition, 1D ZnO is relatively biosafe and biocompatible and can be used for biomedical applications [11]. TiO_2 is also widely used in the synthesis of nanosemiconductor applications such as solar cell and sophisticated electronic optical devices [12, 13]. Mesoporous TiO_2 indicates fairly high activity in photocatalysis performance due to its high specific surface area [14]. A fast and convenient preparation method to obtain TiO_2 with high porosity, high homogeneity and high surface area is required [15]. However, compared with the pure components of TiO_2 and ZnO, TiO_2/ZnO tandem nanostructures show increased photocatalytic performance and enhanced

B. Kılıç (✉) · V. Çelik
Department of Energy Systems Engineering, Faculty of Engineering, Yalova University, 77100 Yalova, Turkey
e-mail: bkilic@yalova.edu.tr; kbayramkilic@gmail.com

photoluminescence (PL) properties [16, 17] due to the high electron injection efficiency of TiO_2 and high electron transport rate and large specific surface area of ZnO [18]. Additionally, TiO_2/ZnO structure limits the recombination of photogenerated electrons by acting as an energy barrier between the photoanode and electrolyte interface [19]. In this study, we investigated the physical, thermal and optoelectronic properties of the TiO_2/ZnO tandem structures. The study is mainly focused on the rational synthesis, structure analysis and novel properties of TiO_2/ZnO tandem structures which can be used in optoelectronic devices. Various methods have been described for the preparation of ZnO nanostructures including metal organic chemical vapor deposition, vapor–liquid–solid, chemical vapor deposition, pulsed laser deposition, electrochemical deposition, hydrothermal process and template-based methods [20, 21]. Among these methods, hydrothermal method is a promising technique and does not require expensive equipment, complex process control and high growth temperature. This method not only allows growing ZnO nanostructures at low temperature (50–200 °C), but also provides large-scale production [22].

2 Experimental procedure

2.1 Materials

Conducting glasses with fluorine-doped SnO_2 (FTO $\sim$14 Ω/cm^2) were used as the substrate. Firstly, the substrates were cleaned carefully by dipping for 2 min each in Propan-2-ol, deionized water, methanol and deionized water, in sequentially manner. The FTO substrates were cut into lots of pieces with a dimension of 2 cm × 2 cm. The pieces were ultrasonically cleaned with trichloroethylene, acetone, methanol and deionized water. Titanium (IV) oxide and $Zn(NO_3)_2{\cdot}6H_2O$ (aq) were used for the synthesis of the hybrid photoanodes. The pH was adjusted by a concentrated solution of ammonia (28 %, Sigma-Aldrich).

2.2 Design of tandem nanostructures based on TiO_2 mesoporous/ZnO nanowire

The tandem nanostructures based on TiO_2 mesoporous/ZnO nanowires were fabricated as follows. First, aqueous solution of 1 mM titania (IV) oxide, 10 ml HCl and 40 ml deionized water were prepared into Teflon-lined stainless steel autoclave. Eight milliliters of ammonia (28 %) was added into the solution for adjusted pH >4.5. FTO substrates were immersed into the solution and then heated to 175 °C for 24 h. After hydrothermal processes, the substrate was dried by N_2 blowing. As a result, the TiO_2 mesoporous was obtained on FTO substrates and sample was placed in a furnace at 450 °C for 40 min in order to remove of defects. When we changed molar ratio of solution from 1 to 10 mM titania (IV) oxide, we obtained different amount mesoporous TiO_2 on FTO substrate about TiK Wt = 3.99 and 15.83 %, respectively. Secondly, 1D ZnO nanowires arrays were grown within mesoporous TiO_2 substrate. 1 mM $Zn(NO_3)_2{\cdot}6H_2O$ (aq) solution was prepared, and pH of the solution was adjusted to $\sim$11 using ammonia solution. Then, the mesoporous TiO_2 substrates were immersed into the solution and then heated to 150 °C for 16 h. The final products of all samples were annealed in air at 450 °C for 1 h so as to use structural and optical characterization.

2.3 Characterization of tandem nanostructures based on TiO_2 mesoporous/ZnO nanowires thin films

The surface morphology of the tandem nanostructures was analyzed using a The Philips XL30 ESEM-FEG/EDAX system (SEM-EDAX). The crystal structure was analyzed by X-ray diffraction (XRD) (Rigaku D/Max-IIIC diffractometer) with Cu–Kα radiation of 1.54 Å, within the 2θ angle ranging from 20° to 80°. The absorption measurements were carried out by Perkin-Elmer UV–VIS Lambda 2S spectrometer. The PL measurements were conducted with the RF 5301 PC Shimadzu spectrofluorometer at room temperature. Thermal decomposition temperatures of TiO_2/ZnO nanostructures were measured by Simultaneous TGA-DTG Instrument (SEIKO). The surface composition, which is capable of providing atomic and molecular information regarding the surface of the material, was investigated by X-ray photoelectron spectroscopy (XPS: Thermo Scientific K-Alpha X-ray Photoelectron Spectrometer is used). The Raman scattering measurements were taken using a micro Raman Renishhaw 2000 system with an excitation source of 514.5 nm at room temperature.

3 Results and discussion

3.1 Morphology and structural properties of tandem TiO_2 mesoporous/ZnO nanowires structures

Figure 1a–d shows scanning electron microscopy (SEM) images and XRD patterns of as-synthesized TiO_2 mesoporous, ZnO nanowires and TiO_2/ZnO tandem nanostructures. The surface morphology, crystal structure and orientation of TiO_2 mesoporous are shown in Fig. 1a. The SEM image shows that the TiO_2 mesoporous are homogenously grown on FTO substrate by hydrothermal method. It can be seen that the TiO_2 mesoporous have 50–100 nm pore radius and 2 μm film thickness. The phase purity and orientation of the TiO_2 mesoporous are shown

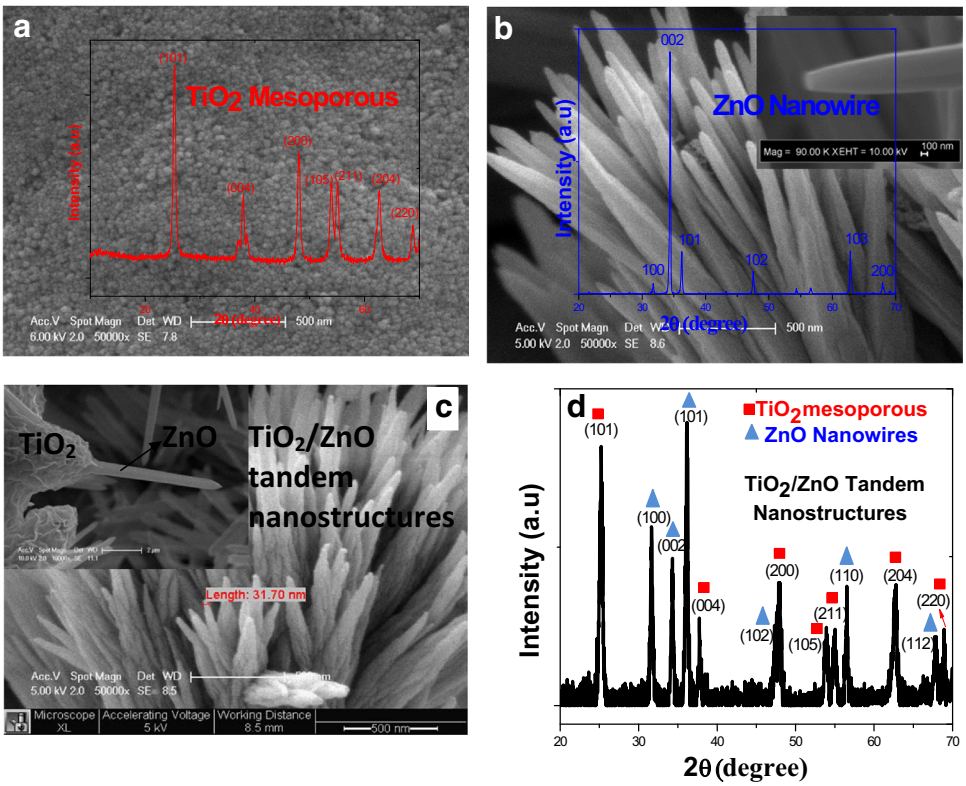

Fig. 1 SEM images and XRD pattern of **a** TiO_2 mesoporous, **b** ZnO nanowires, **c** SEM images of TiO_2/ZnO tandem structures and **d** XRD pattern of TiO_2/ZnO tandem structures

on SEM images in Fig. 1a. XRD characterizations explain that the pure TiO_2 can be well indexed to anatase structure (JCPDS No. 65-5714) without any impurity diffraction peaks. Good crystallization is also shown from sharp diffraction peaks. The mesoporous crystalline structures show an anatase phase with preferred (101) orientation at $2\theta = 25.25^{\circ}$. All other diffraction peaks at (004), (200), (105), (211), (204) and (220) are assigned well to anatase crystalline phase of TiO_2 mesoporous structures. In addition, high-ordered ZnO nanowire structures are also obtained on FTO substrate due to attempt to make a one-to-one comparison of structural and optical characterization with TiO_2 mesoporous and TiO_2/ZnO tandem nanostructures. The SEM images in Fig. 1b indicate a high density and homogeneous distribution of the ZnO nanowires can be growth on the FTO substrate. The SEM images also showed that the ZnO nanowires have average diameter in the range of 30–50 nm, and their lengths are several tens of microns. The synthesized ZnO nanowires were analyzed with XRD patterns to determine the crystallinity and crystal planes of the as-grown structures. As can be seen in Fig. 1b, all diffraction peaks are consistent with the values of the standard (JCPDS card No. 36-1451), and the nanowires show the pure hexagonal ZnO structure with high crystallinity. The peaks at $2\theta \approx 31.64^{\circ}$, 34.46° and 36.23° are attributed to (100), (002) and (101) ZnO planes, respectively. The enhanced (002) diffraction peak at $2\theta \approx 34.46^{0}$ indicates the preferential orientation of the crystals along the *c*-axis of the ZnO nanowires. The surface and typical cross-section morphology of TiO_2/ZnO tandem structures are shown in Fig. 1c. It can be clearly seen that the ZnO nanowires have been successfully and uniformly grown within the TiO_2 films after the hydrothermal reaction, forming a tandem film consisting of ZnO nanowires and TiO_2 mesoporous structures with TiK Wt = 3.99 and 15.83 % for 1 and 10 mM titania (IV) oxide, respectively. It is also revealed that the VA ZnO NWs are well-grown with a uniform morphology within the TiO_2 substrates. The average diameters and lengths of the as-grown ZnO NWs were normally in the range of 50–100 nm and above 10 μm with dense arrays. Interestingly, the use of pH (arranged with the ammonia %28) of $Zn(NO_3)_2{\cdot}6H_2O$ (aq) seeding on the TiO_2-coated FTO substrate is the essential step for synthesizing highly branched ZnO NWs. The TiO_2/ZnO tandem film maintains the mesoporous structure of the TiO_2 film, indicating the postinjecting of ZnO nanowires does not induce any degradation of the TiO_2 film structures. XRD characterization shows that the diffraction peaks of both anatase TiO_2 and wurtzite ZnO could be observed in the as-prepared tandem structures, implying that the films consist of TiO_2 and ZnO (Fig. 1d) and there is no other impurity phase from the XRD diffraction peaks. The average crystalline sizes of above three samples calculated using the diffraction peaks (1 0 1)

of anatase phase for TiO_2 or wurtzite phase for ZnO from Scherer's formula [19] are in the range of 15–30 nm.

EDX analysis result can give the chemical composition of the TiO_2/ZnO tandem films. As shown in Fig. 2a, b, the peaks of O, Zn and Ti can be clearly seen while no other elements are detected besides those Au doped because Au element is used on samples in order to increase conductivity of the films. The amount of TiO_2 mesoporous in film can be adjusted by varying the Ti-precursor concentration. Because of the concentrations of 1 mM titania (IV) oxide are increased to 10 mM titania (IV) oxide, similar contents of Ti element are indicated at 3.99 wt% and 15.83 wt% in TiO_2/ZnO tandem structure, respectively. The Ti element distribution is similar to that of Zn and O elements in both modified ZnO nanowires. Considering the small size of TiO_2 nanoparticle or TiO_2 mesoporous observed in SEM image (Fig. 1), it is hard for EDX image to locate Ti element exactly. But the overall Ti element distributions in both samples suggest that the TiO_2 mesoporous structure is well distributed below ZnO nanowires

The XPS analysis is investigated to show presence of TiO_2 and ZnO oxide phases in the hybrid films, which is in accordance with XRD analysis. XPS spectrums of TiO_2/ZnO tandem films are shown in Fig. 2c, d respectively. The peak positions were referenced to carbon at 285 eV. In Fig. 2c, the XPS peaks with binding energies of 1,020.86 and 531.41 eV correspond to Zn $2p_{3/2}$ and O 1*s*, respectively. TiO_2/ZnO tandem film shows an additional peak with a binding energy of 473.501 eV corresponding to Ti $2p_{3/2}$ is present in Fig. 2c. This is due to the formation of Ti^{3+}. In hybrid films of TiO_2/ZnO, the strong chemical activity of Ti^{3+} can transfer excessive electrons to the carboxylate group of the dye molecules, which forms coordination bonding and may increase the amount of dye adsorption [23]. Moreover, the formation of Ti^{3+} can increase oxygen vacancies, which support the transport of electrons and holes between dye molecules and the photoanode [24]. The Ti 2p peak of TiO_2/ZnO tandem shifts to a lower banding energy. It also shows that coated ZnO can change the energy band of TiO_2. The peak position of the film prepared with TiO_2/ZnO is shifted to a high binding energy due to the O 1*s* band position at higher binding energy in TiO_2 compared with that in ZnO. Figure 2d shows the narrow scan of Zn 2p which confirm the presence of peaks with a binding energy of 1,020.86 and 1,043.99 eV corresponding to Zn 2p3/2 and Zn 2p1/2, respectively.

3.2 Optical characterization of TiO_2/ZnO hybrid structures

The UV–Vis spectra of TiO_2 mesoporous, ZnO nanowires and TiO_2/ZnO hybrid structures with a wavelength range of 300–800 nm are presented in Fig. 3. As can be seen that pure TiO_2 show absorption spectra consisting a single sharp absorption at around 397 nm which is in good agreement with the band gap value of anatase (Fig. 3). This absorption edges of TiO_2 mesoporous occurred at

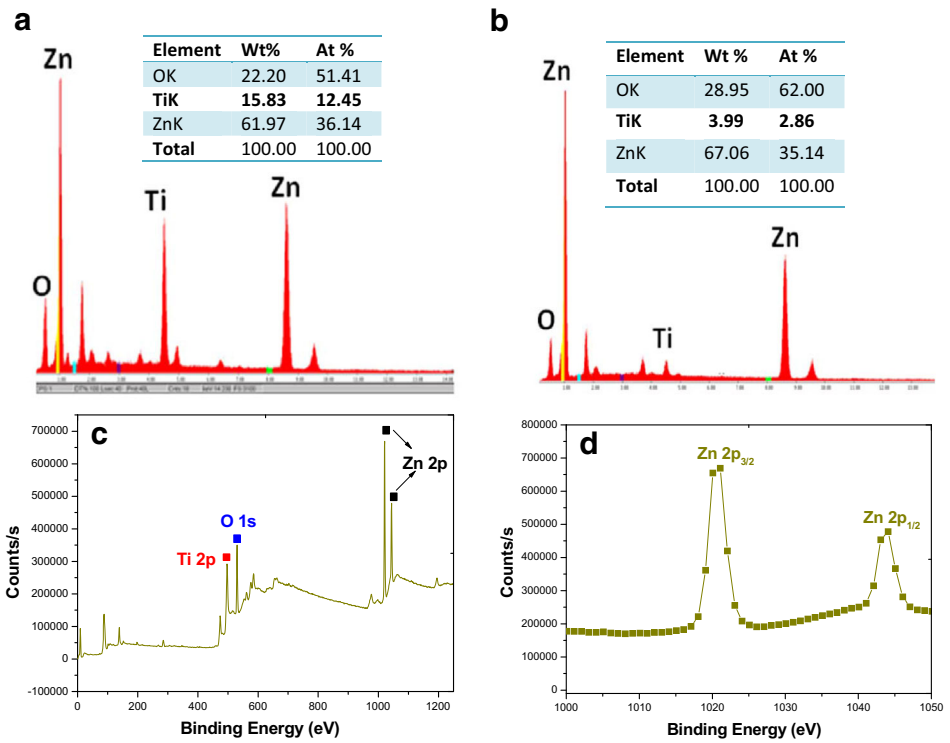

Fig. 2 **a**, **b** EDAX measurements of TiO_2/ZnO tandem structures with different amount of TiO_2 mesoporous. XPS of TiO_2/ZnO tandem structures. **c** The wide scan range and **d** the Zn 2p level peak

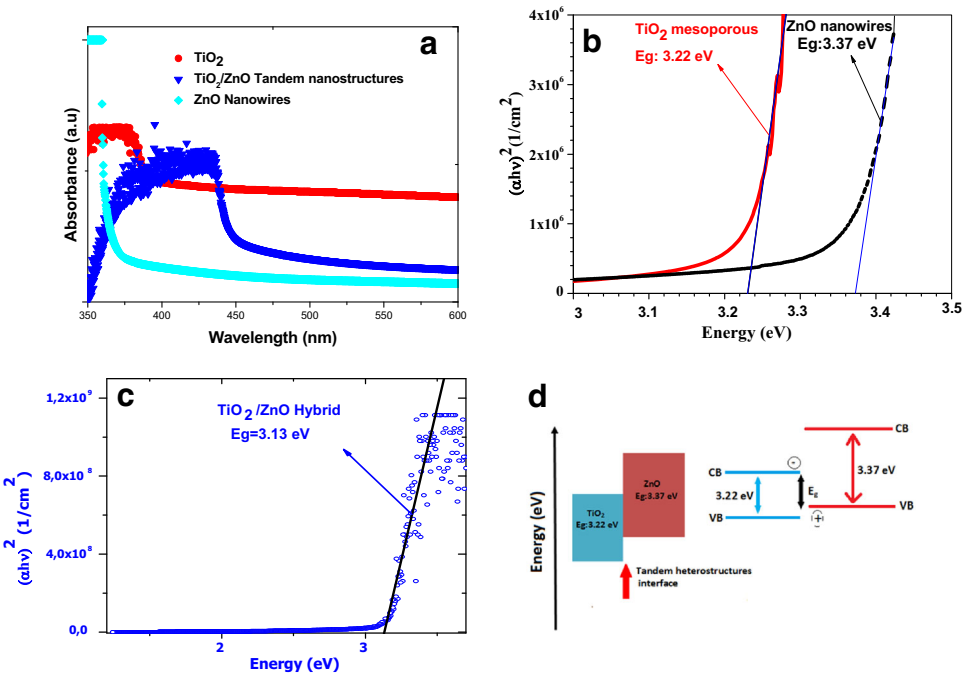

Fig. 3 Absorbance spectrum of **a** TiO_2 mesoporous, ZnO nanowires and TiO_2/ZnO tandem structures, **b-c** Absorption coefficient/energy plot of TiO_2, ZnO and TiO_2/ZnO tandem structures at room temperature, **d** Schematic illustration of Energy band diagram for TiO_2/ZnO tandem structures

$\lambda = 397$ nm due to the charge transfer from the valance band which is mainly formed by $2p$ orbitals of the oxide anions to the conduction band which is mainly formed by $3d$ t_{2g} orbitals of TiO^{4+} cations [22–24], whereas the absorption spectra of ZnO nanowires show a well-known exciton band and strong blueshift compared mesoporous TiO_2 from Fig. 3a, b. This blueshift is mainly due to quantum confinement effect of the ZnO nanowires. Between 365 and 420 nm, a weak absorption band is explained below the band gap that may be related to defects levels. UV–Vis spectra indicated that an obvious redshift compared with TiO_2 mesoporous, possibly due to differences in the surface state of the ZnO/TiO_2 tandem structures (Fig. 3c, d). From the UV–Visible spectrum, optical band gap can be calculated by the following equation [25]:

$$(\alpha h\nu) = A\,(h\nu - E_g)^{1/2}$$

where α is absorption coefficient and A is constant. The direct band gap E_g was determined from $(\alpha h\nu)^2$ photon energy, and as a result, optical band gap was calculated as 3.22, 3.37 and 3.13 eV for TiO_2 mesoporous, ZnO nanowires and TiO_2/ZnO hybrid structure, respectively. It was indicated that the band energy of TiO_2/ZnO hybrid structure is lower than that for ZnO nanowires and TiO_2 mesoporous. The presence of ZnO can modify the optical properties, to extend the range of the excited spectrum and favor the absorption of solar energy in the visible region.

Figure 4a illustrates the PL spectra of mesoporous TiO_2, ZnO nanowire and TiO_2/ZnO tandem film under room temperature. ZnO nanowire shows a strong ultraviolet luminescent band at 361 nm (3.4 eV), and it is commonly believed that the ultraviolet emission band is due to the recombination of free excitons between conductive band and valence band of ZnO nanowires and is called near-band-edge emission. The broad emission peaking at 2.65 eV (blue) in the ZnO nanowire samples might be due to deep level(s), which is also shown clearly in the absorption measurement at very similar energy values. However, TiO_2 mesoporous does not show an obvious UV luminescence corresponding to the near-band-edge (NBE) emission due to its indirect-band energy structure [26]. The PL spectrum of TiO_2 mesoporous film shows a weak and broad green emission band. PL spectrum of TiO_2 mesoporous indicates self-trapped excitons, oxygen vacancies and surface states. The peak of green emission band at about 540 nm is attributed to oxygen vacancy, and these oxygen vacancies are at the surface of TiO_2 [27]. The PL spectra of TiO_2/ZnO tandem structures show that the UV, violet and yellow emission peaks appeared at 3.1, 2.6 and 2.3 eV, respectively. It was shown that two different green emission peaks appeared at 469 and 531 nm. The green emission peak at 469 nm was stronger than the UV luminescence at 394 nm in the samples. These results confirm that the PL of the ZnO/TiO_2 hybrid structure is mainly determined by the electrons in the conduction band owing to the higher barrier in the valence band preventing the hole's movement [28, 29].

Figure 4b shows the schematic diagram of the enhanced PL processes for TiO_2/ZnO tandem structures with Raman scattering spectra measurements. In semiconductors, the electrons and holes are at their lowest energy states. The enhanced ultraviolet emission of ZnO/TiO_2 tandem

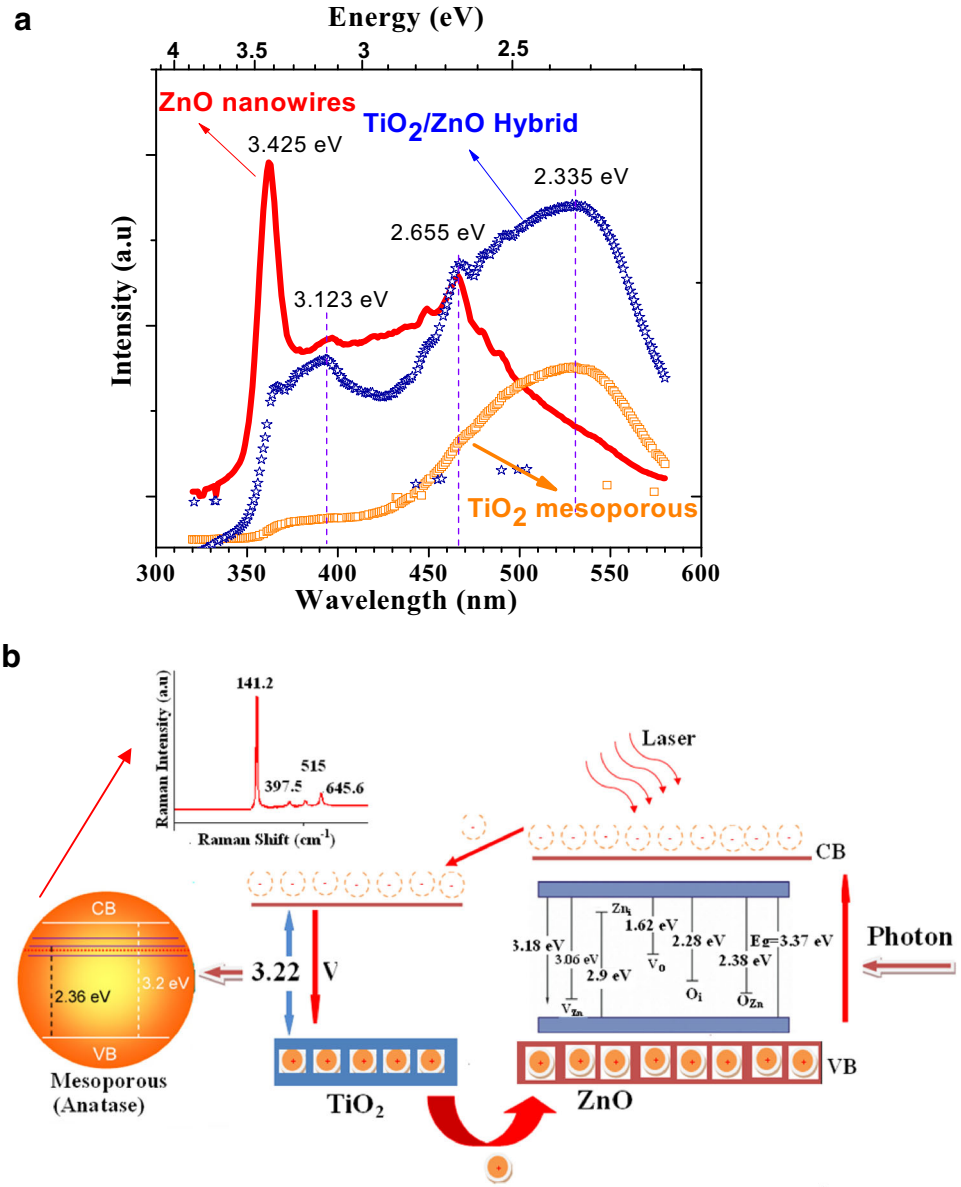

Fig. 4 Room temperature photoluminescence (PL) spectrum of TiO_2 mesoporous, ZnO nanowires and TiO_2/ZnO tandem structures **b** Illustration of photoinduced charge transfer and separation at the TiO_2/ZnO tandem structures and Raman spectra

structures is related to the fluorescence resonance energy transfer between TiO_2 mesoporous and ZnO nanowires [30, 31]. The energy variation at the interfaces of hybrid structures tends to spatially separate those electrons and holes which are excited by UV light on different sides of the ZnO nanowires and TiO_2 mesoporous hetero-junction [32]. The energy band gap of TiO_2 mesoporous structures is located at 3.2 eV between valance band and conduction band. Both energy levels are covered by 1D ZnO nanowires. As shown in Fig. 5b, under illumination of TiO_2/ZnO hybrid samples, the electrons easily go down from the conduction band of ZnO nanowire to conduction band of TiO_2 mesoporous. In addition, the holes are passed from the valence band (VB) of TiO_2 to VB of ZnO. The excited electron–hole pairs are made up in TiO_2 mesoporous structures, as usual; they can recombine through the band edge as well defect states when the incident photon energy is below the band gap energy of ZnO nanowires [30]. It was shown that the atomic flat interfaces across TiO_2 and ZnO of TiO_2/ZnO tandem structures ease this charge transfer/isolation process by a decreased interface resistance [30, 31]. In addition, the 1D ZnO nanowires may also helps to decrease the recombination probability of photogenerated carriers due to an increased delocalization of electrons [31]. To investigate the crystal quality and structural defect of TiO_2/ZnO tandem structures, Raman spectra were also carried out at room temperature. Raman scattering spectrum clearly identifies the anatase phase of the TiO_2 mesoporous on the basis of its Raman band at 141.2 cm^{-1} of E_g mode [32]. It is known that the E_g mode

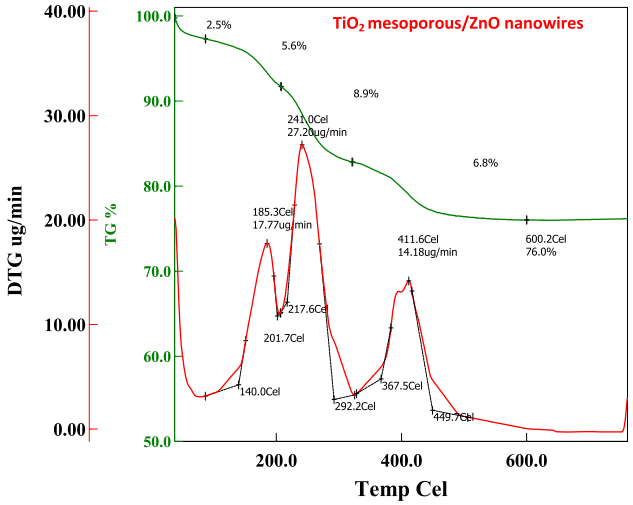

Fig. 5 TGA and DTG results of TiO_2/ZnO tandem structures

corresponds to O–Ti–O bending-type vibration. The lack of other peaks characterized rutile and brookite phases suggests that the TiO_2 has a pure anatase phase. A small peak at about 397 cm^{-1} is observed from the spectra and is attributed to be the A1T modes of ZnO. The presence of this peak is due to impurities and structural defect of oxygen vacancies and Zn interstitials [33].

3.3 Thermal characterization of TiO_2/ZnO hybrid structures

Thermogravimetry is one of the most widely used techniques to observe the composition and structural dependence on the thermal degradation of a hybrid or composite structures. Figure 5 shows the results of thermogravimetry analyses (TGA and DTG) of the TiO_2/ZnO tandem structures. The thermogravimetric analysis (TGA) and the derivative thermogravimetric measurements (DTG) of the samples are shown in figure in order to investigate thermal stability. TGA from room temperature to 800 °C was conducted to identify the thermal stability and the amount of TiO_2/ZnO tandem structures. The weight loss below 20 °C reflects the loss of humidity and acid. As shown in Fig. 5, TGA curve of TiO_2/ZnO exhibits a typical interlayer water loss up to 180 °C. Rapid mass loss (2.5 %) up to 135 °C is followed by slower mass loss approaching a constant value toward the end of thermal dehydration at 180 °C. At this temperature, mass loss of 5.6 % was observed for hybrid structures. The 8.9 % weight loss between 200 and 400 °C was attributed to the elimination of OH groups from the structure. TGA measurements of TiO_2/ZnO tandem structures can imply a formation of low-concentration oxygen vacancies during the heat treatment, due to the escape of part of the crystal lattice oxygen from the component single oxides (ZnO, TiO_2). The DTG analysis shows an initial peak between 150 and 200 °C with a weight loss of up to 17.7 %, which was related to moisture evaporation. After this peak, DTG shows one sharp peak and one small peak in the range of 200–500 °C. These three peaks may arise from the loss of chemical bonding water. A strong peak started at 241 °C with the maximum at 260 °C can be found in the DTG curve, it is induced by the thermal decomposition of hybrid chains of TiO_2/ZnO hetero-structures. Consequently, this thermal event also caused a broad exothermic peak in the range of 200–330 °C in the DTA curve (figure not shown). The last sharp DTG peak centered at 411.6 °C accompanied by a strong exothermic peak in the DTA curve should arise from the oxidation decomposition of TiO_2/ZnO tandem structures in the air.

4 Conclusion

One-dimensional (1D) ZnO nanowires has been grown within mesoporous TiO_2 structures for tandem nanosystem design. 1D ZnO nanowires and mesoporous TiO_2 are an important and promising class of nanoscale materials for environment-friendly and cost-effective optoelectronics devices. Hydrothermal methods are successfully used to produce tandem structures. The presence of TiO_2 in the film of TiO2/ZnO tandem structures is confirmed by EDX and XPS. XPS has shown that the mesoporous TiO_2 is anatase. EDX analysis indicates the chemical composition of the TiO_2/ZnO hybrid films. It has been shown that the enhanced ultraviolet emission of ZnO/TiO_2 tandem structures is related to the fluorescence resonance energy transfer between TiO_2 mesoporous and ZnO nanowires.

Acknowledgments This project was supported by The Scientific and Technological Research Council of Turkey (TUBITAK, Project Number: 114F292) and the Research found of Yalova University, Project Number 2013/BAP/085.

References

1. Z. Yunyan, M. Jin, Controllable synthesis of flower-and rod-like ZnO nanostructures by simply tuning the ratio of sodium hydroxide to zinc acetate. Nanotechnology **7**, 075606 (2007)
2. C. Cheng, A. Amini, C. Zhu, Z. Xu, H. Song, N. Wang, Enhanced photocatalytic performance of TiO2–ZnO hybrid nanostructures. Sci. Rep. **4**, 4181 (2014)
3. C. Lao, Y. Li, C.P. Wong, Z.L. Wang, Enhancing the electrical and optoelectronic performance of nanobelt devices by molecular surface functionalization. Nano Lett. **7**(5), 1323–1328 (2007)
4. B. KiliC, L. Wang, O. Ozdemir, M. Lu, S. Tüzemen, One dimensional (1D) ZnO nanowires dye sensitized solar cell. J. Nanosci. Nanotechnol **13**, 333–338 (2013)
5. Y. Tak, S.J. Hong, J.S. Lee, K. Yong, Solution-based synthesis of a CdS nanoparticle/ZnO nanowire heterostructure array. Cryst. Growth Des. **9**(6), 2627–2632 (2009)

6. M.R. Mohammadi, R.R.M. Louca, D.J. Fray, M.E. Welland, Dye-sensitized solar cells based on a single layer deposition of TiO_2 from a new formulation paste and their photovoltaic performance. Sol. Energy **86**(9), 2654–2664 (2012)
7. B. Kılıç, E. Gür, S. Tüzemen, Nanoporous ZnO photoelectrode for dye-sensitized solar cell. J. Nanomater. **7**, 474656 (2012)
8. S.H. Lee, H.J. Lee, H. Goto, M. Cho, T. Yao, Fabrication of Porous ZnO nanostructures and morphology control. Phys Status Solidi C **4**(5), 1747–1750 (2007)
9. Q. Zhang, C.S. Dandeneau, X. Zhou, G. Cao, ZnO nanostructures for dye sensitized solar cell. Adv. Mater. **21**, 4087–4108 (2009)
10. Z.L. Wang, J. Song, Piezoelectric nanogenerators based on zinc oxide nanowire arrays. Science **312**(5771), 242–246 (2006)
11. J. Zhou, N.S. Xu, Z.L. Wang, Dissolving behavior and stability of ZnO wires in biofluids: a study on biodegradability and biocompatibility of ZnO nanostructures. Adv. Mater. **18**(18), 2432–2435 (2006)
12. G. Tang, S. Liu, H. Tang, D. Zhang, C. Li, X. Yang, Template-assisted hydrothermal synthesis and photocatalytic activity of novel TiO_2 hollow nanostructures. Ceram Int. **39**, 4969–4974 (2013)
13. T. Yu, X. Tan, L. Zhao, Y. Yin, P. Chen, J. Wei, Characterization, activity and kinetics of a visible light driven photocatalyst: cerium and nitrogen co-doped TiO_2 nanoparticles. Chem. Eng. J. **157**, 86–92 (2010)
14. S. Kim, D. Kim, H. Choi, M.S. Kang, K. Song, S.O. Kang, J. Ko, Enhanced photovoltaic performances and long-term stability of quasi solid state dye sensitized solar cell via molecular engineering. Chem. Commun. **40**, 4951–4953 (2008)
15. S.H. Kang, J.Y. Kim, Y.Y. Kim, H.S. Kim, Y.E. Sung, Surface modification of stretched TiO_2 nanotubes for solid-state dye-sensitized solar cells. J. Phys. Chem. C **111**, 9614–9623 (2007)
16. J.J. Qiu, F.W. Zhuge, K. Lou, X.M. Li, X.D. Gao, X.Y. Gan, W.D. Yu, H.K. Kim, Y.H. Hwang, A facile route to aligned TiO_2 nanotube arrays on transparent conducting oxide substrates for dye-sensitized solar cells. J. Mater. Chem. **21**, 5062–5068 (2011)
17. K.E. Kim, S.R. Jang, J. Park, R. Vittal, K.J. Kim, Enhancement in the performance of dye-sensitized solar cells containing ZnO-covered TiO_2 electrodes prepared by thermal chemical vapor deposition Sol. Energy Mater. Sol. Cells **91**, 366–370 (2007)
18. T.R. Andersen, T.T. Larsen-Olsen, B. Andreasen, A.P.L. Böttiger, J.E. Carlé, M. Helgesen, E. Bundgaard, K. Norrman, J.W. Andreasen, M. Jørgensen, F.C. Krebs, Aqueous processing of low-band-gap polymer solar cells using roll-to-roll methods. ACS Nano **5**, 4188–4196 (2011)
19. C-Shii Chou, F-Cheng Chou, J-Yuan Kang, Preparation of ZnO-coated TiO_2 electrodes using dip coating and their applications in dye-sensitized solar cells. Powder Technol. **215–216**, 38–45 (2012)
20. C.Y. Jiang, X.W. Sun, G.Q. Lo, D.L. Kwong, J.X. Wang, Improved dye-sensitized solar cells with a ZnO-nanoflower photoanode. Appl. Phys. Lett. **90**(26), 263501–263503 (2007)
21. F. Yueping, P. Qi, W. Xiaogang, W. Jiannong, Y. Shihe, Synthesis of ultrathin ZnO nanofibers aligned on a zinc substrate. Small **2**(5), 612–615 (2006)
22. S. Baruah, J. Dutta, Hydrothermal growth of ZnO nanostructures. Sci. Technol. Adv. Mater. **10**(1), 013001 (2009)
23. N. Wang, X.Y. Li, Y.X. Wang, Y. Hou, X.J. Zou, G.H. Chen, Synthesis of ZnO/TiO_2 nanotube composite film by a two-step route. Mater. Lett. **62**, 3691–3693 (2008)
24. A. Irannejad, K. Janghorban, O.K. Tan, H. Huang, C.K. Lim, P.Y. Tan, X. Fang, C.S. Chua, S. Maleksaeedi, S.M.H. Hejazi, M.M. Shahjamali, M. Ghaffari, Effect of the TiO_2 shell thickness on the dye-sensitized solar cells with $ZnO–TiO_2$ core–shell nanorod electrodes. Electrochim. Acta **58**, 19–24 (2011)
25. Bayram Kilic, Taylan Günes, Ilknur Besirli, Merve Sezginer, Sebahattin Tuzemen, Construction of 3-dimensional ZnO-nanoflower structures for high quantum and photocurrent efficiency in dye sensitized solar cell. Appl. Surf. Sci. **318**, 32–36 (2014)
26. C.W. Zou, X.D. Yan, J. Han, R.Q. Chen, J.M. Bian, E. Haemmerle, W. Gao, Preparation and enhanced photoluminescence property of ordered ZnO/TiO_2 bottlebrush nanostructures. Chem. Phys. Lett. **476**, 84–88 (2009)
27. L. Xu, H. Shen, X. Li, R. Zhu, Influence of annealing temperature on the photoluminescence property of ZnO thin film covered by TiO_2 nanoparticles. J. Lumin. **130**, 2123–2127 (2010)
28. D. Ma, J. Huang, Z. Ye, L. Wang, B. Zhao, Relationship between photoluminescence and structural properties of the sputtered $Zn_{1-x}Cd_xO$ films on Si substrates. Opt. Mater. **25**, 367 (2004)
29. K. Prabakar, C. Kim, C. Lee, UV, violet and blue-green luminescence from RF sputter deposited ZnO: Al thin films. Cryst. Res. Technol. **40**, 1150 (2005)
30. H.Y. Lin, Y.Y. Chou, C.L. Cheng, Y.F. Chen, Giant enhancement of band edge emission based on ZnO/TiO_2 nanocomposites. Opt. Express **15**, 13832 (2007)
31. A. Leelavathi, G. Madrasa, N. Ravishankar, Origin of enhanced photocatalytic activity and photoconduction in high aspect ratio ZnO nanorods. Phys. Chem. Chem. Phys. **15**, 10795–10802 (2013)
32. T. Ohsaka, F. Izumi, Y. Fujiki, Raman spectrum of anatase, TiO_2. J. Raman Spectrosc. **7**, 321–324 (1978)
33. A. Umar, Y.B. Hahn, ZnO nanosheet networks and hexagonal nanodiscs grown on silicon substrate: growth mechanism and structural and optical properties. Nanotechnology **17**, 2174 (2006)